Advances in Water Resources 158 (2021) 104040

Contents lists available at ScienceDirect

Advances in Water Resources

journal homepage: www.elsevier.com/locate/advwatres

Equivalent hydraulic conductivity, connectivity and percolation in 2D and 3D random binary media

Iván Colecchio [a,c], Alejandro D. Otero [b,d], Benoît Noetinger [e,f], Alejandro Boschan [a,c,*]

[a] Grupo de Medios Porosos, Facultad de Ingeniería, Universidad de Buenos Aires, Paseo Colón 850, Buenos Aires, Argentina
[b] Departamento de Energía, Facultad de Ingeniería, Universidad de Buenos Aires, Paseo Colón 850, Buenos Aires, Argentina
[c] CONICET, Buenos Aires, Argentina
[d] Centro de Simulación Computacional, CSC - CONICET, Godoy Cruz 2390, Buenos Aires, Argentina
[e] IFPEN, Direction Earth Sciences and Environmental Technologies, 1 & 4, avenue de Bois-Préau, 92852 Rueil-Malmaison Cedex, France
[f] Department of Thermal Science and Energy Engineering, University of Science and Technology of China, Hefei, Anhui 230026, China

ARTICLE INFO

Keywords:
Percolation
Up-scaling
Binary media
Stochastic

ABSTRACT

The equivalent hydraulic conductivity (K_{eq}) relates the spatial averages of flux and head gradient in a block of heterogeneous media. In this article, we study the influence of connectivity on K_{eq} of media samples composed of a high conductivity (k^+) and a low conductivity (k^-) facies. The k^+ facies is characterized by a proportion p, and also by two connectivity parameters: a connectivity structure type (no, low, intermediate, high), and a correlation integral scale l_c.

The probability distribution of K_{eq}, and the critical value of p at which percolation occurs (p_{av}), are studied as a function of these connectivity parameters. The distribution of $\log(K_{eq})$ is Gaussian in all cases, so the results are presented in terms of the geometric mean ($\langle K_{eq}\rangle$) and the variance ($\sigma^2_{\log(K_{eq})}$).

Both quantities show a data collapse if expressed as a function of $p - p_{av}$ (for the variance $\sigma^2_{\log(K_{eq})}$, notably, even if 2D and 3D data are plotted together). In 3D, when a connectivity structure exists, K_{eq} is always greater than when no structure exists, and increases (while p_{av} decreases) as l_c increases. The same is observed in 2D, except for the low connectivity structure type (i.e. when the k^+ facies is disconnected), that shows an unprecedented behaviour: K_{eq} is greater in the absence of structure, and decreases (p_{av} increases) as l_c increases. Our results show that any influence of connectivity on K_{eq} is well accounted for simply by a shift in the percolation threshold p_{av}, and then, suggest that K_{eq} is controlled mainly by the proximity to percolation.

1. Introduction

1.1. Equivalent conductivity and connectivity

Achieving a precise description of the equivalent hydraulic conductivity (K_{eq}) of heterogeneous media is of great interest in several subsurface related disciplines, such as ground water management, waste disposal, CO2 storage and hydrocarbon applications. The homogenization procedure that makes it possible to derive a representative K_{eq} value over a certain block, from the point conductivity values $k(\mathbf{r})$, is termed upscaling. The equivalent conductivity K_{eq} tends to the effective conductivity K_{eff} as the size of the block tends to infinity (Dagan et al., 2013).

Frequently, the scarcity of field data in subsurface-related applications is mitigated by the use of a geostatistical stochastic approach (Gelhar, 1986; Linde et al., 2015; Godoy et al., 2018). In this approach, uncertainty is addressed by generating independent realizations of a sample of a subsurface formation. For simplicity, let's consider a sample of linear size L and volume L^D, where D is the space dimensionality. The point conductivity $k(\mathbf{r})$ is defined over a regular Cartesian grid of linear cell size Δ. In each sample, $k(\mathbf{r})$ is considered to be a random process characterized by a probability density function $P(k(\mathbf{r}))$, and the spatial variation of $k(\mathbf{r})$ is defined by a covariance function with a certain integral length scale (l_c). Eventually, the realizations can be conditioned with the available field data. For lognormal media, the mean and variance of $P(k(\mathbf{r}))$ may suffice to determine K_{eq}, with a small influence of the type of covariance function in 3D (De Wit, 1995). However, in certain scenarios, for example if tortuous channels are present, it has

* Corresponding author at: Grupo de Medios Porosos, Facultad de Ingeniería, Universidad de Buenos Aires, Paseo Colón 850, Buenos Aires, Argentina.
E-mail address: abosch@fi.uba.ar (A. Boschan).

https://doi.org/10.1016/j.advwatres.2021.104040
Received 12 March 2021; Received in revised form 19 August 2021; Accepted 10 September 2021
Available online 15 September 2021

been shown (Western et al., 2001) that additional information regarding the spatial organization of $k(\mathbf{r})$ is required.

This motivated an important number of studies that explored connectivity as the source of such information. In a first group of studies, Zinn and Harvey (2003), and later Jankovic et al. (2017), modified multigaussian continuous fields (for which intermediate $k(\mathbf{r})$ classes are naturally connected, while the extreme $k(\mathbf{r})$ classes are disconnected), by applying a Normal Score Transform to swap the intermediate $k(\mathbf{r})$ classes with the high (or the low) ones. This made it possible to increase (or reduce) the connectivity of the high $k(\mathbf{r})$ classes, without changing $P(k(\mathbf{r}))$ or the spatial covariance function of $k(\mathbf{r})$. In these studies, connectivity was explored through different configurations arising from the reorganization of the $k(\mathbf{r})$ classes, and through the covariance function. It was shown that the ratio between the K_{eq} of the connected structure to that of the disconnected one can, notably, reach a value of 10 in 2D while it decreases to 2.2 in 3D (both for high variances). This shows the strong effect of dimensionality.

In a second group, other authors evaluated new ways to describe and measure connectivity, or analyzed how connectivity metrics are correlated to K_{eq}. Some of them studied continuous $k(\mathbf{r})$ fields (Masihi et al., 2016; Tyukhova and Willmann, 2016), while others considered multi-facies media, with a discrete distribution of $k(\mathbf{r})$ values (Nurafza et al., 2006; Fleckenstein and Fogg, 2008; Vassena et al., 2010; Rongier et al., 2016). In all cases, it is concluded that measuring the connectivity of the high $k(\mathbf{r})$ classes is crucial to assess groundwater flow.

1.2. Upscaling and percolation in binary media

A binary medium (Knudby et al., 2006; King et al., 2001) has a proportion p of a high conductivity facies ($k(\mathbf{r}) = k^+ = \text{constant}$) and a proportion $(1-p)$ of a low conductivity facies ($k(\mathbf{r}) = k^- = \text{constant}$). It is a simplified representation of multi-facies media that makes it possible to retain salient geometrical heterogeneity features (Hunt and Idriss, 2009; Zarlenga and Fiori, 2015), while rendering the parameter space more tractable. Nevertheless, binary media may accurately model natural formations (Guin and Ritzi, 2008), for example, in sandstone-shale or sand-clay mixtures. Their study constitutes a gateway to understand the percolative behaviour of K_{eq} in multi-facies models. Regarding their flow properties, a distinctive feature is a sharp increase of K_{eq} when p overcomes the percolation threshold p_c, i.e, when it appears a spanning cluster in the k^+ facies (a k^+ cluster) connecting the sample along the mean flow direction (Hunt and Idriss, 2009).

Analytical methods to estimate K_{eq} in binary media were developed, in general, on the basis of effective medium theory and perturbation methods (Maxwell, 1873; Dagan, 1989; Pozdniakov and Tsang, 2004). Hashin and Shtrikman (1962) showed that, for binary isotropic media, and without taking into account the spatial organization of the facies, K_{eq} lies in a bounded range narrower than the one set by the arithmetic and harmonic averages (Wiener, 1912). Bernabé et al. (2004) provided a simple model for statistical isotropic and infinite media that enables the estimation of K_{eq} in the framework of percolation theory. In this model, for $p < p_c$, the media is assumed to be composed by isolated inclusions of the k^+ facies randomly distributed in a matrix of the k^- facies, so K_{eq} is estimated as the Hashin-Shtrikman lower bound (Eq. (1)).

$$K_{eq} = k^- + \frac{p}{\frac{1}{k^+ - k^-} + \frac{1-p}{3k^-}} \quad ; \quad p < p_c. \tag{1}$$

For $p > p_c$, K_{eq} is mainly controlled by the proportion p^* of the volume of the spanning cluster (with $p^* < p$) to the total sample volume. In this case, the media is considered as formed by two facies: k^+, with proportion p^*, and a second (fictitious) one, with characteristic conductivity k_M ($k^+ > k_M > k^-$) and proportion $(1-p^*)$. The latter is a mixture arising from the combination of the k^- facies and the component of the k^+ facies that don't belong to the spanning cluster. The conductivity k_M is obtained with Eq. (1), but using $(p-p^*)/(1-p^*)$ as the relative proportion of the k^+ facies in the mixture. An estimation of p^* can be obtained using the power-law in $(p-p_c)$ from percolation theory (Stauffer and Aharony, 1994). Finally, K_{eq} is computed using the Hashin-Shtrikman upper bound as Eq. (2):

$$K_{eq} = k^+ + \frac{1-p^*}{\frac{1}{k_M - k^+} + \frac{p^*}{3k^+}} \quad ; \quad p > p_c. \tag{2}$$

Later, Oriani and Renard (2014) improved the model of Bernabé et al. (2004) by characterizing the spanning cluster via image analysis, and correcting the value of p^* using the convex hull of the clusters. This model drops the statistical isotropy requirement, and has no size restrictions, resulting in a more accurate estimation, but is more expensive in terms of computing time, especially in 3D.

As explained above, as many flow features are determined by the connectivity of the k^+ facies (Nurafza et al., 2006), a percolative analysis is of interest for accurate flow modelling and K_{eq} estimation. In this regard, we highlight three important issues:

1. The existence of a spatial correlation of $k(\mathbf{r})$, characterized by the integral scale l_c, affects the connectivity, as it modifies the size of the k^+ clusters. Previous works (Harter, 2005; Guin and Ritzi, 2008) have shown that an increase of l_c leads to a decrease of p_c. Also, we recall that, keeping all other variables constant, an increase of l_c typically implies an increase of K_{eq} (Paleologos et al., 1996; Boschan and Noetinger, 2012).
2. Percolation thresholds vary significantly between 2D and 3D. Also, in 2D isotropic binary media, only one percolating facies can exist, while this restriction does not exist in 3D (Neuweiler and Vogel, 2007; Zarlenga et al., 2018). It becomes evident that dimensionality will strongly affect any connectivity characterization. Moreover, several connectivity indicators are borrowed from percolation theory (Stauffer and Aharony, 1994; Hunt, 1998; Renard and Allard, 2013).
3. Due to the finite size of the media samples, finite size scaling affects the percolation transition (King et al., 1999). The critical value of p for which percolation occurs for a sample of linear size L (here termed p_{av}) tends to p_c as $L \to \infty$. Also, $k^- > 0$, in contrast with formal percolation theory for which $k^- = 0$. These finite effects may influence K_{eq}, differently for 2D than for 3D.

These facts demonstrate that analyzing connectivity features in 2D and 3D at the same time is important to gain understanding on how connectivity indicators can be used to predict K_{eq}.

1.3. K_{eq} distributions

In the stochastic approach mentioned in Section 1.1, the relative frequency of K_{eq} values in the ensemble of realizations defines a (probability) distribution, i.e. $P(K_{eq})$ (Fenton and Griffiths, 1993; Sanchez-Vila et al., 2006).

This distribution is often represented by its mean value ($\langle K_{eq} \rangle$) (the first gaussian moment) (Knudby et al., 2006; Oriani and Renard, 2014; Liao et al., 2019), and by its variance ($\sigma^2_{\log(K_{eq})}$) (the second gaussian moment), particularly for multigaussian media (Dykaar and Kitanidis, 1992; Attinger, 2003). In the case of binary media, as p approaches p_c, $P(K_{eq})$ may undergo a transition from unimodal to bimodal (with two well-defined modal K_{eq} values, see Fig. 6 in Boschan and Noetinger (2012)). The probability distribution widens, and some values of K_{eq} between the modes may have negligible relative frequency (a gap appears in $P(K_{eq})$). In those cases, it is necessary to carefully evaluate if $P(K_{eq})$ is appropriately described by only $\langle K_{eq} \rangle$ (and eventually by $\sigma^2_{\log(K_{eq})}$ also).

Depicting the shape of $P(K_{eq})$ is then of key importance to gain conceptual understanding of the underlying flow situation, particularly on the onset of a percolative behaviour, with direct impact in uncer-

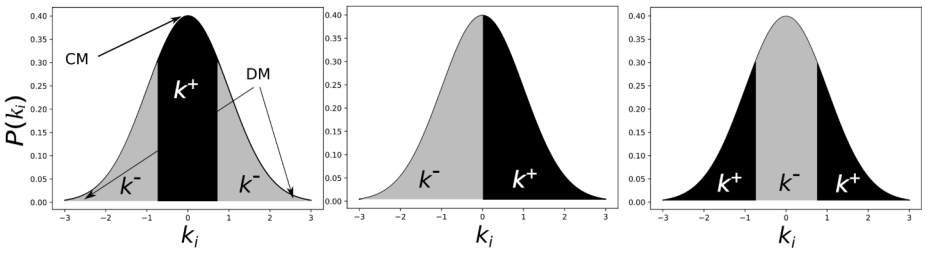

Fig. 1. Schematics of the truncation procedure used to obtain the target binary samples from underlying multigaussian ones. These examples have $p = 0.5$, the black areas correspond to the k^+ facies while the gray ones correspond to the k^- facies. (Left): high; (center): intermediate; and (right): low connectivity structure types. Note that in the underlying multigaussian samples, intermediate $k_i(\mathbf{r})$ values form a connected matrix (CM), while the extreme values form a disconnected matrix (DM).

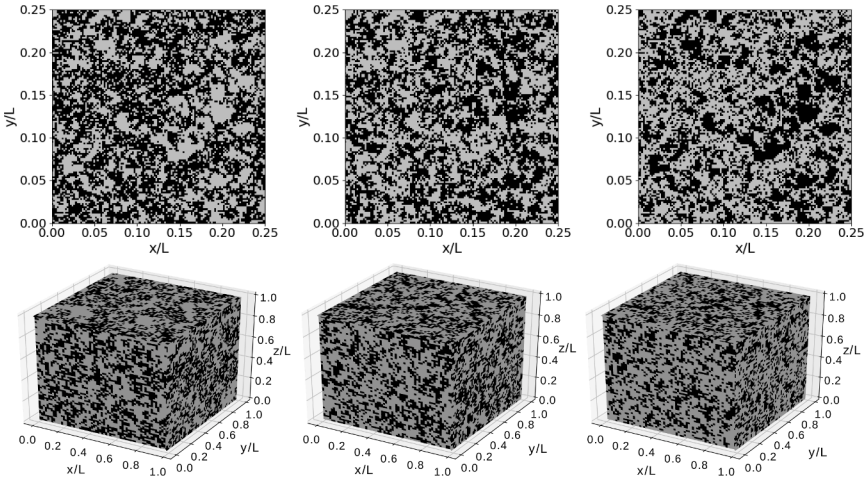

Fig. 2. Maps of $k(\mathbf{r})$ for the binary samples used in the present study. (Black): k^+, (gray): k^-. (Top): 2D binary samples (only a part of them is shown for clarity), with $p = 0.5$ and $l_c = 3\Delta$. (Bottom): 3D binary samples, with $p = 0.4$ and $l_c = 2\Delta$. (Left): high; (center): intermediate; and (right): low connectivity structure types.

tainty management applications. Moreover, the influence of connectivity on $P(K_{eq})$ becomes of interest, and to our knowledge, has not yet been addressed in the literature.

1.4. Objectives

The objective of this paper is to analyze the interplay among connectivity, percolation and $P(K_{eq})$ of saturated isotropic binary media. We have decided to carry out the study both in 2D and 3D, aiming to provide a better understanding of the subtle extrapolation from 2D to 3D, and also to obtain insight over the potentially complex behaviour of $P(K_{eq})$ in 3D. To this end, we have constructed random binary media samples with no, low, intermediate, or high connectivity structure type, in a binary media version of the procedure followed by previous authors (Zinn and Harvey, 2003; Jankovic et al., 2017; Zarlenga et al., 2018) using continuous $k(\mathbf{r})$ fields. The use of binary media makes it possible to analyze how connectivity influences K_{eq} from the point of view of percolation. We intend to portray here a wide range of connectivity scenarios. Connectivity was varied explicitly by changing the connectivity structure type and the integral scale l_c (these are the connectivity parameters that control the spatial organization of the k^+ facies), but also implicitly by varying the proportion p of the k^+ facies. Media samples with $l_c \to 0$ are used to represent the lack of structure. In Section 2 we present the numerical methodology employed to construct the binary samples (FFT-MA generator, Le Ravalec et al. (2000)), to use cluster analysis to determine the percolation threshold p_c (CONNECT3D, Pardo-Igúzquiza and Dowd (2003)), and to compute K_{eq} (MODFLOW-2005, Harbaugh (2005)).

The results are presented in Section 3, where we first examine the distributions $P(K_{eq})$ for the different connectivity structure types. Then, the behaviour of the first two gaussian moments of $P(K_{eq})$, the mean $\langle K_{eq} \rangle$ and the variance $\sigma^2_{\log(K_{eq})}$, is studied as a function of p, l_c, and the connectivity structure type.

Later, it is shown that the influence of l_c and of the connectivity structure type on $\langle K_{eq} \rangle$ and $\sigma^2_{\log(K_{eq})}$ is well accounted for simply by a shift in the percolation threshold p_{av}. Finally, we present a final discussion and outline the perspectives for future work.

2. Numerical methodology

The first step (described in Section 2.1) of our stochastic approach consisted in generating square (2D) or cubic (3D) binary media samples. The k^+ facies of the samples are characterized by three parameters: a connectivity structure type (no, low, intermediate, high), an integral scale l_c, and a proportion p. Then, $k(\mathbf{r})$ was upscaled from the fine scale Δ to the scale L of the sample size (which is constant in this work), obtaining one K_{eq} value for each realization (Section 2.2). Finally, we have used a cluster identification function to estimate p_{av} for each value of l_c, and each connectivity structure type (Section 2.3).

2.1. Generation of binary fields with different connectivity structure types

The binary media samples were obtained by the following procedure:

a. Generation of multigaussian media samples, with a standard normal distribution of an intermediate indicator $k_i(\mathbf{r})$, using an isotropic exponential covariance function. These will be referred to as underlying (multigaussian) media samples. As explained in Section 1.1, for these, intermediate $k_i(\mathbf{r})$ classes form a connected matrix, while the extreme $k_i(\mathbf{r})$ classes form a disconnected matrix. Random field generation was performed using a fast Fourier transform (FFT) moving average (FFT-MA) method (Le Ravalec et al., 2000).
b. Binarization by truncation, mapping the $k_i(\mathbf{r})$ point values from the multigaussian samples onto k^+ or k^- point values in the target binary samples. The truncation schemes shown in Fig. 1 were used to

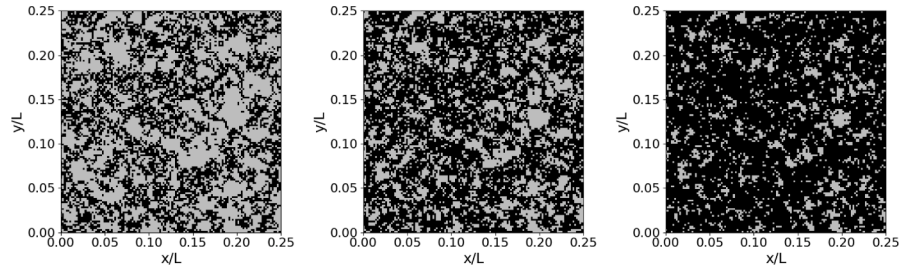

Fig. 3. 2D binary samples (only a part of them is shown for clarity), $l_c = 3\Delta$, with a high connectivity structure type. (Black): k^+, (gray): k^-. (Left): $p = 0.4$, (center): $p = 0.6$, (right): $p = 0.8$. When the proportion p is small, the connected matrix is populated by the k^+ facies, but, as p increases, the disconnected matrix also becomes gradually occupied by the k^+ facies.

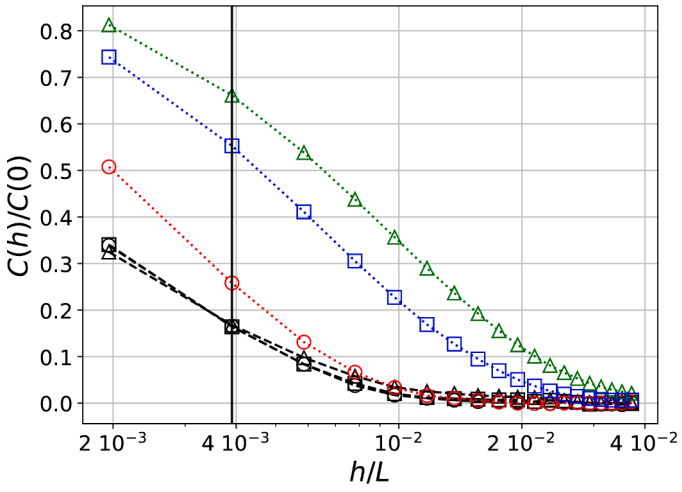

Fig. 4. Covariance of $k(\mathbf{r})$, as a function of the lag distance h /L, for 2D binary samples (- - -) with $p = 0.4$ and $l_c = 3\Delta$ (indicated by the vertical line). (△): High; (○): intermediate; (□): low connectivity structure types. The covariance functions of the multigaussian samples used to construct the binary samples of each connectivity structure type are indicated by (····) and the corresponding coloured marker: (△): High; (○): intermediate, (□): low connectivity structure types.

generate binary media samples with high, intermediate or low connectivity structure types (Fig. 2).

For the high connectivity structure type, when the proportion p is small, the connected matrix of the underlying multigaussian sample (this is, the intermediate $k_i(\mathbf{r})$ classes, for which the indicator takes values close to zero), becomes the k^+ facies after binarization. But, as p increases, also the disconnected matrix of the underlying multigaussian sample (the extreme $k_i(\mathbf{r})$ classes) gradually becomes part of the k^+ facies of the binary samples. This is illustrated in Fig. 3, where binary media samples of the high connectivity structure type are shown for different values of p. For the low connectivity structure type, when the proportion p is small, the connected matrix of the underlying multigaussian sample becomes the k^- facies in the binary samples (and the disconnected matrix becomes the k^+ facies). But, as p increases, the disconnected matrix of the underlying multigaussian sample also becomes gradually part of the k^- facies in the binary samples. The intermediate connectivity structure type is obtained by performing a standard truncation over the multigaussian samples (Allard, 1993). These truncation procedures are depicted in Fig. 1.

Depending on the connectivity structure type, one or two (equal but with opposite signs) cutoff indicator values are required to control the proportion p of the k^+ facies in the binary samples.

Fig. 2 shows examples of the resulting binary media in 2D (top, $p = 0.5$) and 3D (bottom, $p = 0.4$). A sample with a high (low) connectivity

Table 1
Simulation parameter symbols, descriptions and values.

Description	Symbol	Values	
		2D	3D
Grid cell size (m)	Δ	1	
Size of samples	L	512 Δ	64 Δ
Integral scale	l_c	$0.001\Delta; 2\Delta; 3\Delta$	$0.001\Delta; 1.5\Delta; 2\Delta$
Facies conductivity (m/day)	k^+, k^-	100, 0.01	
k^+ facies proportion	p	$[0.4, \ldots, 0.8]$	$[0.1, \ldots, 0.5]$
Connectivity structure type	–	High, low, intermediate	

structure type is constituted by blobs of the k^- (k^+) facies embedded in a k^+ (k^-) matrix. For the intermediate connectivity structure type, neither of the facies embeds the other.

We have verified that the binarization procedure described in step (b) maintains the exponential nature of the covariance function, while l_c changes, depending on the value of p, and on the connectivity structure type. The exponential covariance is defined in Eq. (3), where h is the lag or distance between two points, l_c is the correlation integral scale, and $C(0)$ is the variance of $P(k(\mathbf{r}))$.

$$C(h) = C(0)\exp\left(-\frac{3h}{l_c}\right) \tag{3}$$

For the intermediate connectivity structure type, an analytical relation between the integral scales of the gaussian and of the binary media can be found in Mariethoz and Caers (2014). We are not aware of an analogous formula for the high and low connectivity structure types. Because of this, and to compare binary media with the same covariance function but different connectivity structure types, it was necessary to map the value of l_c of the multigaussian samples onto that of the binarized ones. The relation between covariances before and after binarization is depicted in Fig. 4 for the 2D case, where the covariance function for the three connectivity structure types for $p = 0.4$ are shown, along with the ones of the underlying gaussian samples. Note that the value of l_c of the multigaussian sample required to obtain a given l_c of the binarized one depends on the connectivity structure type.

Spatially uncorrelated media samples ($l_c = 0.001\Delta$) were used as a reference of media with no connectivity structure (i.e., at the scale of the sample size). Note that media samples of the three connectivity structure types defined above should statistically coincide as $l_c \to 0$, converging to this reference (uncorrelated) case. Also, due to the small l_c/L ratio, it is reasonable to assume that the ergodic hypothesis holds.

Aiming to study the percolation transition in detail, we have explored 20 values of p in the ranges [0.4; 0.8] for 2D and [0.1; 0.5] for 3D, having in mind that the theoretical values for media with negligible integral scale ($l_c \to 0$), verified in this work, are 0.593 in 2D and 0.312 in 3D (site percolation).

We remark that the sample construction procedure presented here is analogous to the technique conceived by Zinn and Harvey (2003), in that it makes it possible to control the spatial organization of the high $k(\mathbf{r})$ classes while leaving the other parameters unchanged.

The contrast between the characteristic conductivity values for the high and low conductivity facies is 10^4 ($k^+ = 100\ m/day$, $k^- = 0.01\ m/day$). This choice is in line with the proposed percolative approach. In the following, it will be assumed that K_{eq} is made dimensionless by a factor of 1 m/day.

The sample sizes are $L = 512\Delta$ and $L = 64\Delta$ for 2D and 3D respectively, and the values of l_c are 2Δ and 3Δ for 2D, and 1.5Δ and 2Δ for 3D. This choice aimed to equate the statistical sampling between 2D and 3D by matching the number of independent heterogeneity units, that can be estimated as $(l_c/L)^D$ (Boschan and Noetinger, 2012). In Table 1, the main parameters and variables are presented.

To study $\langle K_{eq}\rangle$ and $\sigma^2_{\log(K_{eq})}$ (Section 3.2), we have performed 1000 realizations for each set of parameters (p, l_c, connectivity structure type), while 5000 realizations were performed to achieve a satisfactory resolution for $P(K_{eq})$.

2.2. Computation of K_{eq}

The effective conductivity was computed in the square or cubic domain according to the classic permeameter definition. In this approach, a hydraulic gradient is imposed between inlet (H_{in}) and outlet (H_{out}) faces (Dirichlet boundary conditions), while other boundaries are impervious (Neumann boundary conditions). The flow simulations were performed using MODFLOW-2005[1] software (Harbaugh, 2005), that applies the finite difference method to discretize the Laplace equation. In this scheme, the nodes are located at the center of each square or cubic cell and flow takes place only between adjacent faces. The harmonic mean approximation was used to compute the transmisibilities between adjacent cells Romeu and Noetinger (1995) (1-D flow approximation). The PCG (preconditioned conjugate gradient) was chosen to solve the resulting linear system. Once the flow is solved, we obtain K_{eq} in the mean flow direction as:

$$K_{eq} = \frac{qL}{H_{in} - H_{out}} \tag{4}$$

Where q is the average velocity of the flow through a plane perpendicular to the imposed hydraulic gradient ($(H_{in} - H_{out})/L$). We mention that the samples used in the present study are isotropic as an ensemble (despite the possible statistical fluctuations among individual realizations). The equivalent conductivity K_{eq} can then be well described by using a scalar.

2.3. Cluster analysis and percolation threshold

Two cells were considered as connected only if they shared a face, consistently with the 1-D flow approximation used to compute K_{eq}. The CONNECT3D code (Pardo-Igúzquiza and Dowd, 2003) was used to identify and label the k^+ clusters in each realization (i.e. obtaining a cluster identification function). The code outputs a connectivity metric (N_p) that takes unity value if there exists at least one k^+ spanning cluster connecting the inlet and outlet faces of the sample, and zero otherwise (i.e. it measures connectivity in the mean flow direction). From now on, realizations for which $N_p = 1$ will be referred to as percolating realizations, while those for which $N_p = 0$, as non-percolating realizations.

Taking into account the stochastic approach, the ensemble mean $\langle N_p\rangle$ measures frequency of occurrence of percolation. Moreover, for each connectivity structure type and l_c, the value of p for which $\langle N_p\rangle = 0.5$ (Harter, 2005), (this is, when exactly half of the realizations percolate) was obtained by performing an iterative search. In the following, this critical p value will be referred to as p_{av}, an average percolation threshold. It should not be considered a connectivity indicator, because it cannot be directly measured for any given media sample, but, as it is determined by analyzing N_p (which is indeed a connectivity indicator (Renard and Allard, 2013)), it provides useful connectivity information in the percolation framework. The term p_c will refer to the percolation threshold of infinite media. In Appendix A, the dependence of p_{av} with the domain size L, and its convergence to p_c as $L\to\infty$, are analyzed.

The use of the indicator N_p made it possible to obtain $P(K_{eq})$ separately for the ensembles of percolating and non-percolating realizations. On the other hand, for each realization, the relative proportion p^* of the spanning cluster was explicitly calculated, and then used in the equations proposed by Bernabé (Eqs. (1) and (2)) to estimate K_{eq}.

3. Results and discussion

As discussed in Section 1.3, in certain scenarios, particularly for binary media, it is necessary to assess if $\langle K_{eq}\rangle$ and $\sigma^2_{\log(K_{eq})}$ suffice to provide an accurate description of $P(K_{eq})$. In this regard, we first examine $P(K_{eq})$, analyzing briefly the influence of the connectivity structure type on it. Secondly, we study the $\langle K_{eq}\rangle$ and $\sigma^2_{\log(K_{eq})}$ as a function of p, with the connectivity structure type and l_c as parameters. Finally, we analyze how p_{av} reflects the influence of these parameters on K_{eq}.

3.1. Analysis of the distribution $P(K_{eq})$

For ease of visualization and characterization of the distributions, we'll present results in terms of $P(\log(K_{eq}))$. Figure 5 shows the latter for 2D ($p = 0.566$, $l_c = 0.001\Delta$ and $l_c = 2\Delta$) and 3D ($p = 0.247$, $l_c = 0.001\Delta$ and $l_c = 1.5\Delta$). The values of p are chosen so that, both in 2D and 3D, $\langle N_p\rangle$ equals 0.5 for the intermediate connectivity structure type (this is, just at percolation with $p = p_{av}$). It is observed that, in all cases, $P(\log(K_{eq}))$ can be fitted satisfactorily by a gaussian function, suggesting a lognormal distribution of K_{eq}. When $p = 0$ or $p = 1$, the media are homogeneous and $\log(K_{eq})$ is equal to $\log(k^-)$ or $\log(k^+)$ respectively. In 2D, $\langle N_p\rangle = 1$ and $\langle N_p\rangle = 0$ for the high and low connectivity structure types respectively. In 3D, $\langle N_p\rangle = 0.8$ and $\langle N_p\rangle = 0.1$ for the high and low connectivity structure types respectively. For both, 2D and 3D, $\langle N_p\rangle = 0$ for the no structure case ($l_c = 0.001\Delta$). The distributions of percolating and non-percolating realizations are shown separately for the intermediate connectivity structure type. Note that there are a number of non-percolating realizations with greater K_{eq} values than those of percolating ones, with a considerable overlap between both distributions. In other words, all parameters kept constant, the occurrence of percolation does not imply a higher K_{eq}.

As discussed in Colecchio et al. (2020), for binary media, $P(K_{eq})$ typically undergoes an homogenization from bimodal to unimodal as the linear size of the sample L increases. As p approaches p_{av}, the value of L required to achieve such homogenization increases. We have verified that the distribution $P(K_{eq})$ is unimodal for all the values of p and l_c studied in this work, notably even at $p = p_{av}$, implying that, for the chosen sample size L, the above mentioned homogenization is attained. Comparing the results in terms of the connectivity structure types, in 2D, the distributions $P(K_{eq})$ for $l_c = 2\Delta$ are clearly separated but, there is an overlap between $P(K_{eq})$ of the low connectivity structure type and that of the no structure ($l_c = 0.001\Delta$). In 3D, the distributions for $l_c = 1.5\Delta$ are closer to each other and an overlap does exist between the high connectivity structure type and the intermediate one. Note that the probability distributions for the no structure case and the low connectivity structure case invert their relative positions in 2D with respect to 3D.

[1] https://water.usgs.gov/ogw/modflow/mf2005.html

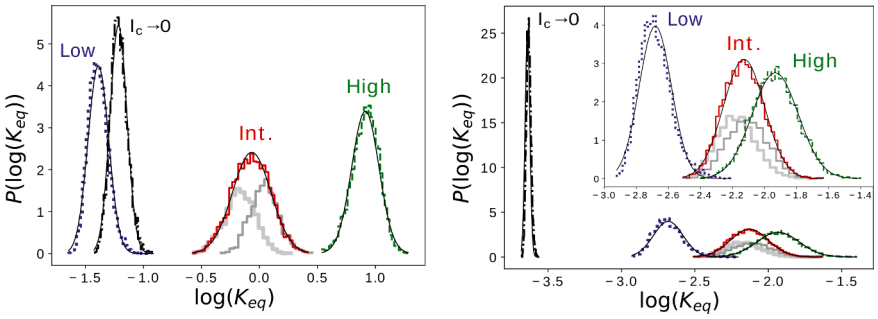

Fig. 5. Probability distributions $P(\log(K_{eq}))$. (Left): 2D at $p = 0.566$ and $l_c = 2\Delta$. (Right): 3D at $p = 0.247$ and $l_c = 1.5\Delta$. For both: (- · - · -): $l_c = 0.001\Delta$ (no structure). (····): Low connectivity structure type. (- -): High connectivity structure type. The values of p are chosen so that, for the case of the intermediate connectivity structure type (——), half of the realizations percolate ($\langle N_p \rangle = 0.5$) while the other half do not. Their distributions corresponding to each half are depicted in dark and light gray lines respectively. (——): Fits by a gaussian function. Inset: Detail of the distributions for 3D media with low, high and intermediate connectivity structure types.

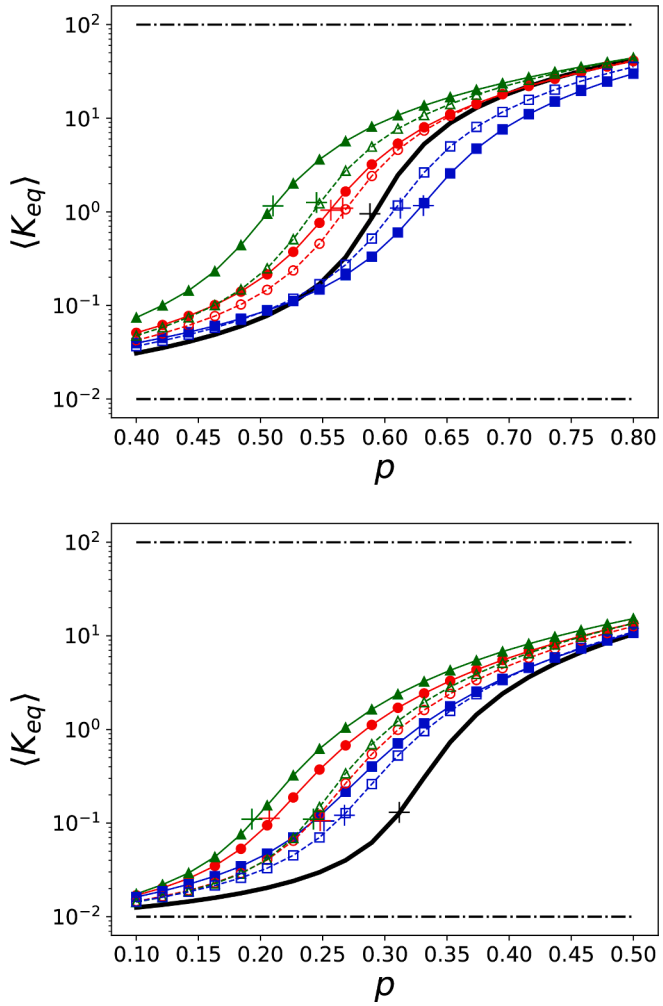

Fig. 6. Mean $\langle K_{eq} \rangle$ as a function of p. (Top): 2D media, (- - -): $l_c = 2\Delta$; and (——): $l_c = 3\Delta$. (Bottom): 3D media, (- - -): $l_c = 1.5\Delta$; and (——): $l_c = 2\Delta$. For both: (△, ▲): High; (○, ●): Intermediate; and (□, ■): Low connectivity structure type. (——): $l_c = 0.001\Delta$ (no structure). The (+) signs indicate, for each trend, the critical p value at which percolation occurs ($\langle N_p \rangle = 0.5$). (- · - · -): $k^- = 0.01\ m/day$, $k^+ = 100\ m/day$. For a given l_c, K_{eq} is always greater for the high connectivity structure type and smaller for the low connectivity structure type. For the same connectivity structure type, a greater l_c implies a greater K_{eq}, except for the low connectivity structure type in 2D. Also, notably, in 2D, but not in 3D, $\langle K_{eq} \rangle$ may be smaller for the low connectivity structure type than when no structure exists.

3.2. Analysis of the first two gaussian moments, the mean $\langle K_{eq} \rangle$ and the variance $\sigma^2_{\log(K_{eq})}$

Figure 6 shows the variation of the geometric mean of K_{eq} (noted $\langle K_{eq} \rangle$) as a function of p. As p approaches the percolation transition, there is a sharp increase of $\langle K_{eq} \rangle$ (Hunt and Sahimi, 2017). However, this increase is smeared-out due to the finite effects mentioned in Section 1.2. In the percolation region, $\langle K_{eq} \rangle$ depends strongly on the connectivity structure type. As an example, in 2D, the values of K_{eq} for the high connectivity structure type can be 30 times greater than those for the low connectivity structure type. In 3D, this ratio reaches a value of 5. These results can be compared with similar ones for lognormal media: 10 for 2D (Zinn and Harvey, 2003), 2.2 for 3D (Jankovic et al., 2017).

The difference among the values of $\langle K_{eq} \rangle$ for the different connectivity structure types is smaller for the lower l_c (2Δ in 2D and 1.5Δ in 3D). On the other hand, $\langle K_{eq} \rangle$ increases as l_c increases in all cases, except, notably, for the low connectivity structure type in 2D, for which it decreases. This may be due to a more efficient isolation of the k^+ clusters, or, in terms of the flow structure, and given the imposed boundary conditions, to a higher fraction of the flow paths being affected by head losses (involving greater energy dissipation). A more detailed discussion is presented at the summary (Section 4). The increase of $\langle K_{eq} \rangle$ with l_c was observed in previous works (Paleologos et al., 1996; Boschan and Noetinger, 2012), and may be related to the dependence of p_{av} with l_c (Harter, 2005), which will be discussed in the next section.

Fig. 7 shows the variance $\sigma^2_{\log(K_{eq})}$, normalized by the variance of $k(\mathbf{r})$ ($\sigma^2_{\log(k)}$), as a function of p. A bell-like shape is always observed, the maxima are located at different values of p. Note that the maximum for $l_c = 0.001\Delta$ is located at 0.593 in 2D and at 0.312 in 3D, the values of p_c for a square (2D) or cubic (3D) lattice (Stauffer and Aharony, 1994).

In all cases, the variance $\sigma^2_{\log(K_{eq})}$ increases as l_c increases (Boschan and Noetinger, 2012). Note that the maximum of $\sigma^2_{\log(K_{eq})}$ increases with l_c, but it is similar for the three types of connectivity structures in 2D, and rather similar in 3D. On the other hand, as l_c increases, the width of the bell increases.

Also, the maximum slope of the curves in Fig. 6 and the position of the maximum in Fig. 7 are related to the occurrence of percolation (Boschan and Noetinger, 2012).

3.3. Percolation analysis

In this section we focus our attention on the percolative behaviour of K_{eq} and its moments, analyzing the critical value p_{av} (calculated as described in Section 2.3) as a function of the integral scale l_c and the connectivity structure type.

Figure 8 shows the fraction of percolating realizations ($\langle N_p \rangle$) as a function of p. Close to p_{av}, $\langle N_p \rangle$ increases steeply from 0 to 1. An initial

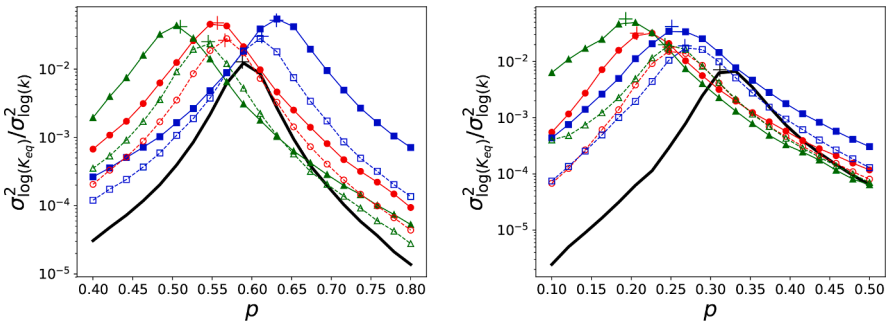

Fig. 7. Normalized variance of $\log(K_{eq})$ as a function of p. (Left): 2D media, (- - -): $l_c = 2\Delta$; and (——): $l_c = 3\Delta$. (Right): 3D media, (- - -): $l_c = 1.5\Delta$; and (——): $l_c = 2\Delta$. For both: (△, ▲): High; (○, ●): Intermediate; and (□, ■): Low connectivity structure type. (——): $l_c = 0.001\Delta$ (no structure). The (+) signs indicate, for each trend, the critical p value at which percolation occurs ($\langle N_p \rangle = 0.5$).

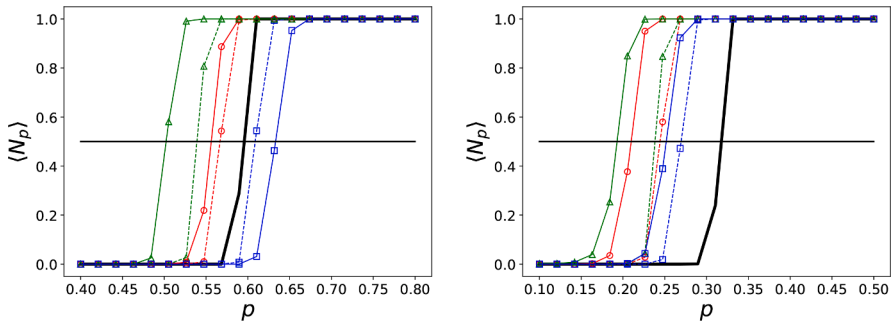

Fig. 8. Fraction of percolating realizations ($\langle N_p \rangle$) as a function of p. (Left): 2D, (····): $l_c = 2\Delta$; and (- - -): $l_c = 3\Delta$. (Right): 3D, (····): $l_c = 1.5\Delta$; and (- - -): $l_c = 2\Delta$. For both: (△): High; (○): Intermediate; and (□): Low connectivity structure type. (——): $l_c = 0.001\Delta$ (no structure).

estimation of p_{av} was obtained from the intersection of the $\langle N_p \rangle$ curves with the horizontal black line ($\langle N_p \rangle = 0.5$). Then, by performing an iterative search, the value of p_{av} for each parameter set was obtained.

Figure 9 shows how p_{av} decreases with l_c, except for the low connectivity structure type in 2D, for which it increases. Here, for the latter case, the interpretation of a more efficient isolation of the k^+ clusters as l_c increases, applies as it did in Fig. 6. The reader should note that an increase of p_{av} with l_c implies that the percolation transition for the 2D low connectivity structure case will occur at a greater value of p than that for the no structure case. This leads to a noticeable result: that introducing spatial correlation may involve a decrease of K_{eq}. This will be further discussed in Section 4. The relationship between p_{av} and l_c shows a rather linear trend for both 2D and 3D. As l_c decreases, the different connectivity structure types converge into a unique uncorrelated structure, and p_{av} tends to the site percolation values for a square (0.593) and cubic (0.312) lattice. The range of values of l_c studied was extended to $l_c = 6\Delta$ in 2D, and to $l_c = 2.5\Delta$ in 3D, to verify the trend.

However, we omitted the analysis of K_{eq} for these extended values of l_c since, in some cases, it was difficult to stabilize the statistical properties of the media and the measured l_c values differed from the input ones. The effect of the fluctuations over the mean values (p_{av}, $\langle K_{eq} \rangle$) is small, but becomes important over the variance $\sigma^2_{\log(K_{eq})}$. On the other hand, in Appendix A, it is shown that the values of p_{av} presented here agree with those of p_c, the asymptotic regime towards $L \to \infty$ being attained.

Figure 10 shows the variation of $\langle K_{eq} \rangle$ with $(p - p_{av})$, using the values of p_{av} from Fig. 9. In this representation, a data collapse is observed, independently of l_c and of the connectivity structure type, and both for 2D and 3D. This implies that a shift in p_{av} suffices to account for any influence of these two connectivity parameters on $\langle K_{eq} \rangle$. Having in mind that the high and low connectivity structure types represent two contrasting connectivity scenarios, this result is noteworthy.

An estimation based on the work of Bernabé et al. (2004) is shown in dashed line (-•-). Here, p^* is computed explicitly for each realization, as described in Section 2.3. For the lower part of the curve, we take into

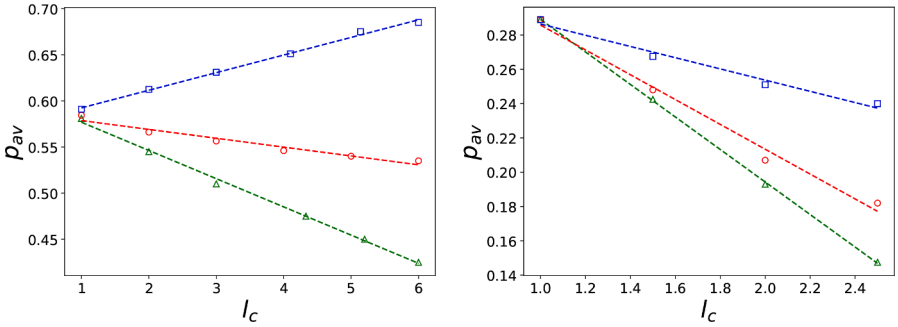

Fig. 9. Average percolation threshold p_{av} as a function of l_c. (Left): 2D media. (Right): 3D media. For both: (△): High; (○): Intermediate; and (□): Low connectivity structure type. The dashed straight lines are guides for the eye. Note that the trends of the three connectivity structure types converge (to the no structure p_{av} value) as $l_c \to 0$.

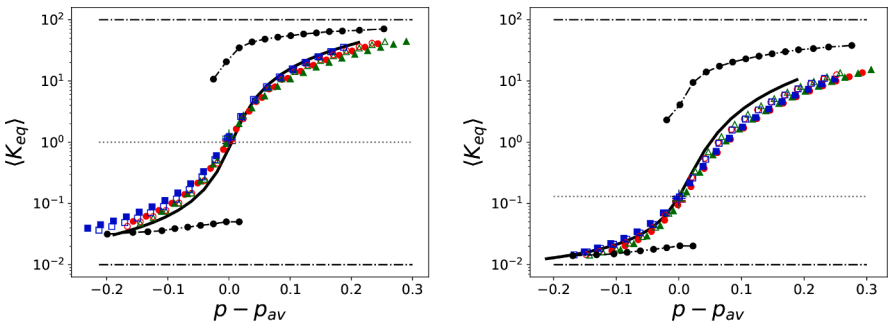

Fig. 10. Mean $\langle K_{eq} \rangle$ as a function of $(p - p_{av})$. (Left): 2D media, (empty markers): $l_c = 2\Delta$ and (solid markers): $l_c = 3\Delta$. (Right): 3D media, (empty markers): $l_c = 1.5\Delta$ and (solid markers): $l_c = 2\Delta$. For both: (△, ▲): High; (○, ●): Intermediate; and (□, ■): Low connectivity structure type. (▬): $l_c = 0.001\Delta$ (no structure). The (+) signs indicate, for each trend, the critical p value at which percolation occurs ($\langle N_p \rangle = 0.5$). (·····): Estimation based on Efros and Shklovskii (1976) for $p = p_{av}$. (-●-): Estimation based on Bernabé et al. (2004). (- - -): $k^- = 0.01\ m/day$, $k^+ = 100\ m/day$. Once the curves are horizontally shifted by the corresponding values of p_{av} (shown in Fig. 9), a collapse is observed. This suggests that the effect of the connectivity parameters over $\langle K_{eq} \rangle$ is mainly a shift or displacement of the percolation threshold.

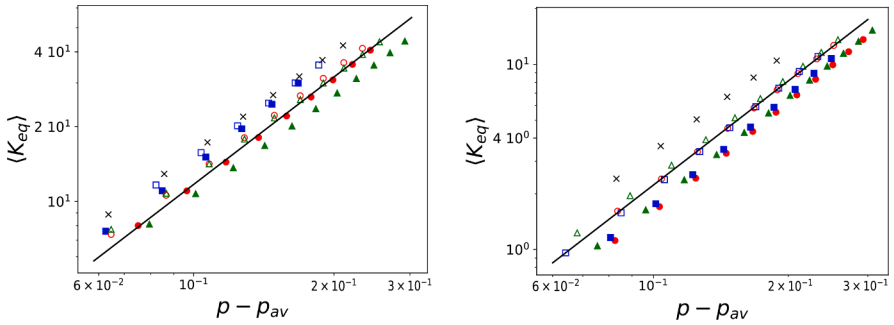

Fig. 11. Mean $\langle K_{eq} \rangle$ as a function of $(p - p_{av})$, for $p > p_{av}$, in log-log scale. (Left): 2D media, (empty markers): $l_c = 2\Delta$ and (solid markers): $l_c = 3\Delta$. (Right): 3D, (empty markers): $l_c = 1.5\Delta$ and (solid markers): $l_c = 2\Delta$. For both: (△, ▲): High; (○, ●): Intermediate; and (□, ■): Low connectivity structure type. (×): $l_c = 0.001\Delta$ (no structure). (▬): Power-law derived from percolation theory using literature values ($\mu = 1.3$ for 2D, and $\mu = 2$ for 3D).

account only the non percolating realizations, using Eq. (1). Likewise, for the upper part of the curve, we use Eq. (2), and consider only the percolating realizations. The estimation predicts an important gap of K_{eq} values for p close to p_{av}, which is not observed in our simulations. In general, the agreement is rather poor in that zone, especially for the 3D case. The difference may arise from the influence of flow dead ends of the spanning cluster, which is simplified in the estimation of Bernabé et al. (2004).

Figure 11 shows $\langle K_{eq} \rangle$ as a function of $(p - p_{av})$, using a log-log scale, for $p > p_{av}$. For comparison, the power-law derived from percolation theory (Eq. (5)) is shown using continuous straight lines, with slopes $\mu =$ 1.3 for 2D, and $\mu = 2$ for 3D, as reported in the literature (Stauffer and Aharony, 1994). When these slopes are obtained by linear fitting over our data, they yield a mean value of $\mu = 1.33$ for 2D and $\mu = 1.9$ for 3D, with little variation among the different connectivity structure types and l_c values.

$$< K_{eq} > \propto (p - p_{av})^{\mu} \tag{5}$$

Regarding the value of K_{eq} at $p = p_{av}$, our results can be contrasted with the finite size scaling predicted for a binary media by Efros and Shklovskii (1976) (Eqs. (6) and (7)). Using the values of high (k^+) and low (k^-) characteristic conductivities employed in our work, this

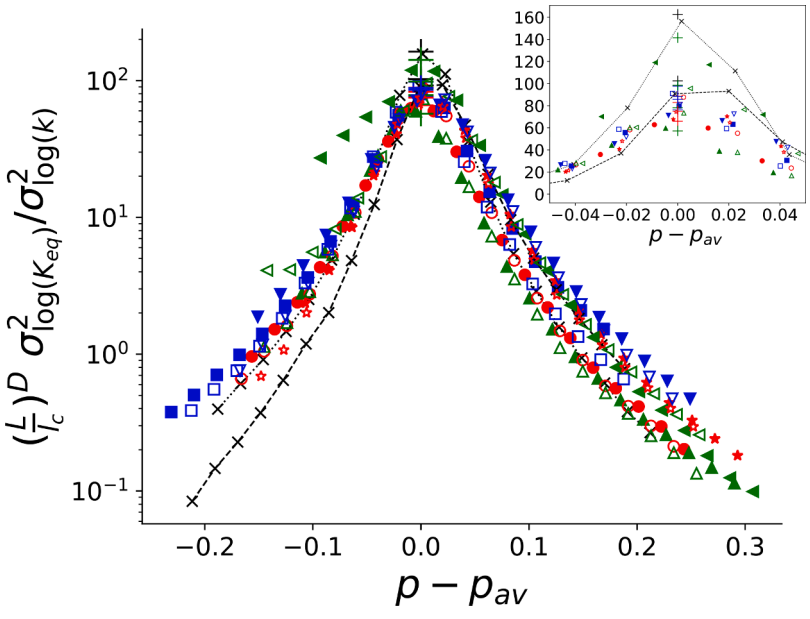

Fig. 12. Data collapse: Normalized variance of $\log(K_{eq})$ (scaled by $(L/l_c)^D$) as a function of $(p - p_{av})$. (Empty markers): $l_c = 2\Delta$ in 2D and $l_c = 1.5\Delta$ in 3D. (Solid markers): $l_c = 3\Delta$ in 2D and $l_c = 2\Delta$ in 3D. (△: 2D / ◁: 3D): High; (○: 2D / ☆: 3D): Intermediate; and (□: 2D / ▽: 3D): Low connectivity structure type. (·····: 2D / - - -: 3D): $l_c = 0.001\Delta$ (no structure). The (+) signs indicate, for each trend, the critical p value at which percolation occurs ($\langle N_p \rangle = 0.5$). (Inset): Detail of the percolation region in linear scale.

prediction yields $K_{eq} = 1$ in 2D and $K_{eq} = 0.13$ in 3D, as:

$$\langle K_{eq} \rangle \simeq \sqrt{k^+ k^-} = 1 \tag{6}$$

and in 3D

$$\langle K_{eq} \rangle \simeq k^+ (k^+/k^-)^{-0.72} = 0.13 \tag{7}$$

On the other hand, from Fig. 6, we obtain $\langle K_{eq} \simeq 1 \rangle$ in 2D, and $\langle K_{eq} \simeq 0.1 \rangle$ in 3D. These results show that $\langle K_{eq} \rangle$ follows a percolative behaviour rather independently of the connectivity parameters. Fig. 12 shows $\sigma^2_{\log(K_{eq})}$, scaled by $(L/l_c)^D$, as a function of $p - p_{av}$. In this representation, it can be observed that the maximum of the $\sigma^2_{\log(K_{eq})}$ (see. Fig. 7) occurs at $p - p_{av} = 0$ in all cases. This result was observed previously by Boschan and Noetinger (2012) and is related to that of Masihi and King (2012) who found that a maximum in the standard deviation of connectivity (quantified by the relative volume of the percolating cluster) occurred at p_c. The scaling factor $(L/l_c)^D$ can be interpreted as the number of the independent heterogeneity units (if $L >> l_c$), making it possible to match the statistical sampling between 2D and 3D. For the cases with $lc = 0.001\Delta$, the variance was scaled by $(L/\Delta)^D$ since the number of the independent heterogeneity units equals the number of cells.

The collapse observed in Fig. 12 is remarkable taking into account that data for 2D and 3D media are plotted together, for all the connectivity structure types and l_c values studied.

4. Summary, conclusions and perspectives

The main result of this paper is that any influence of the studied connectivity parameters on the mean and the variance of K_{eq} is simply reflected in a shift (or displacement) in the percolation threshold p_{av}, both in 2D and 3D. Except for this shift, the dependence of those moments with p is almost identical for all the connectivity scenarios investigated, and follows the scaling predicted by percolation theory.

We reformulate here for 2D and 3D binary media, and then, using a percolative approach, the question posed by Zarlenga et al. (2018) for lognormal continuous media regarding the impact of connectivity for formations sharing the same $P(k(\mathbf{r}))$ and covariance. In terms of parameters, the roles of the connectivity structure type and of the integral scale l_c are conceptually similar in both studies (with the addition of a no structure case in the present one), while the k^+/k^- ratio in binary media plays the role of the variance for lognormal media. However, the proportion p is intimately related to a percolative approach.

Having in mind that the analyzed distributions $P(\log(K_{eq}))$ are always unimodal and Gaussian, and then, well defined by their mean and variance (no information about gaussian moments of higher order is required), the result can be extended in a straightforward manner to the distribution $P(\log(K_{eq}))$ itself.

However, for smaller sample sizes L, $P(\log(K_{eq}))$ may become bimodal (Colecchio et al., 2020), with a greater contrast between percolating and non percolating realizations. In that case, it is not evident if the observed collapse would hold. This remains an open issue and shall be addressed in future works. On the other hand, the validity of the present results for greater sample sizes is analyzed in detail in Appendix A. There, it is shown by extrapolation from a set of smaller subsamples of increasing size that, for the sample size used in this work, p_{av} has already attained its asymptotic behaviour ($L \to \infty$). This suggests that the data collapse observed in Figs. 10 and 12 would hold for largest sample sizes L, and in particular, for $L \to \infty$.

We now focus our attention on the noticeable behaviour of the low connectivity structure type in 2D, for which $\langle K_{eq} \rangle$ decreases (Fig. 6), and p_{av} increases (Fig. 9), as l_c increases, as opposed to all other cases. To our knowledge, this behaviour has never been previously observed in the literature, where it was always found that the appearance of a spatial correlation implied an increase of $\langle K_{eq} \rangle$ (Paleologos et al., 1996; Boschan and Noetinger, 2012) and a decrease of p_{av} (Harter, 2005; Guin and Ritzi, 2008).

This feature may help understanding, from the percolation point of view, why, when comparing media with the same $P(k(\mathbf{r}))$ and covariance function, but different connectivity structure types, a greater contrast of $\langle K_{eq} \rangle$ values may exist in 2D than in 3D. In the work of Zarlenga et al. (2018), it is suggested that this may be originated in a higher probability of existence of a low conductivity barrier extending across the entire sample cross section. In that matter, valuable information is available for binary media: in 2D, only one facies can percolate at a time, while this restriction is not present in 3D (Neuweiler and Vogel, 2007). For example, for the low connectivity structure type, at low values of p, we have indeed verified that the k^- facies forms a spanning cluster, preventing the k^+ facies to do so. In 3D, as p increases, both facies can form a spanning cluster at the same time.

Regarding connectivity and percolation, the percolation threshold has been used in previous works by other authors to measure connectivity for continuous media in the framework of the critical path analysis (Knudby and Carrera, 2005; Masihi et al., 2016). This procedure requires a transformation that consists in adjusting a threshold until a k^+ path spanning the sample appears. Likewise, we acknowledge the limitation arising from the fact that p_{av} cannot be measured for any given media sample. Other connectivity indicators based on statistical measurements of the cluster sizes, such as the average cluster size, or the integral of the connectivity function (Western et al., 2001), were evaluated in the course of the present study, without any significant findings.

Future research should investigate percolation and connectivity on ternary media, to later address more realistic multi-facies models.

Declaration of Competing Interest

The authors declare that they have no known competing financial interests or personal relationships that could have appeared to influence the work reported in this paper.

Acknowledgments

We would like to thank P. Renard and Pardo-Igúzquiza for kind exchanges regarding code implementation, J. Tierno and L. Raineri Marchina for code development. We would also like to acknowledge the computational time from the TUPAC cluster made available by the *CSC-CONICET*, and from M. Saraceno (CIMA-CONICET).

Appendix A. Finite size effects

In this appendix, we analyze how p_{av} behaves for subsamples of linear sizes $\lambda_i < L$, aiming to verify by extrapolation if for the employed sample size L, p_{av} has already attained its asymptotic infinite value p_c, and then, if our results are valid for greater sample sizes. The chosen linear subscales were $\lambda_i = L/2^i$, with $0 \leq i \leq 5$ for both 2D and 3D (i is an integer). For each subsample, $\langle N_p \rangle$ is calculated as shown in Section 2.3.

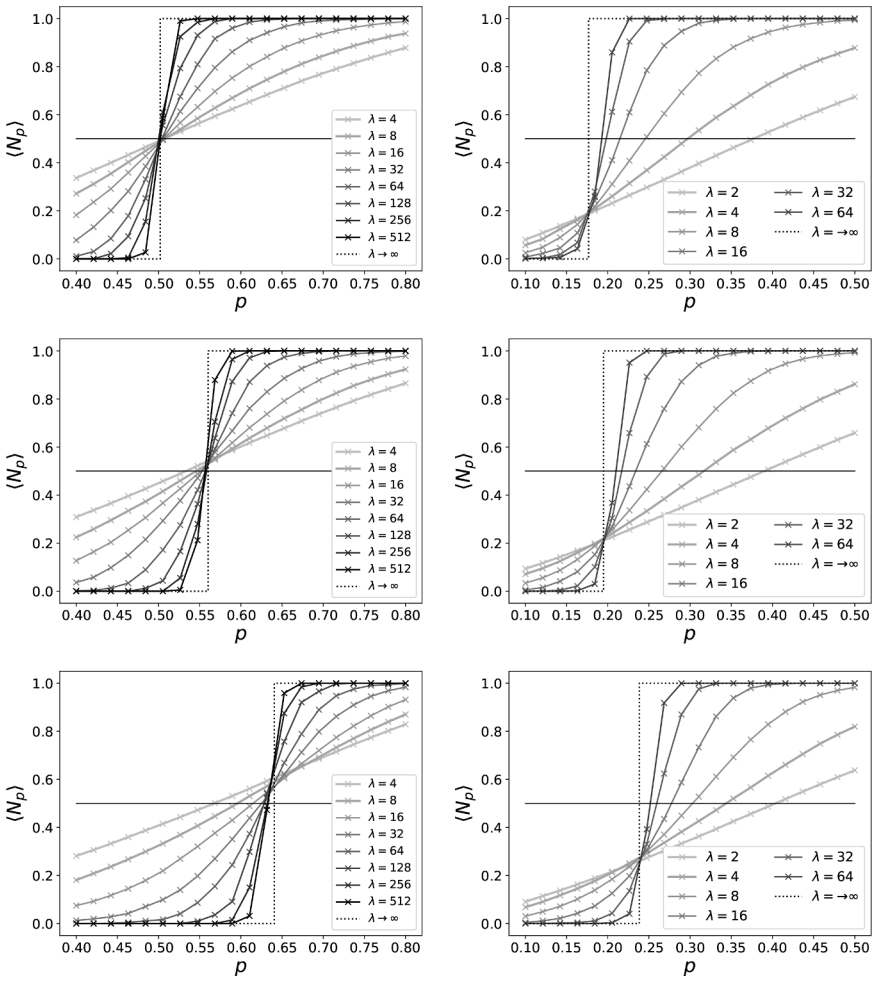

Fig. A1. Fraction of percolating subsamples $\langle N_p \rangle$ for different subscales λ as function of p. (Left): 2D media, $l_c = 3\Delta$. (Right) 3D media, $l_c = 2\Delta$. (Top): High; (Center): Intermediate; and (Bottom): Low connectivity structure type. The dotted line is a representation of the asymptotic value for $\lambda \to \infty$.

Figure A.1 shows the variation of $\langle N_p \rangle$ with p for each λ_i, using $l_c = 3\Delta$ for 2D (left) and $l_c = 2\Delta$ for 3D (right). There is an intersection point common to all the subscales, from which p_c for $L \to \infty$ (⋯) is estimated.

Figure A.2, shows the variation of p_{av} as a function of λ, estimated by interpolating the value of p for which $\langle N_p \rangle = 0.5$ (full horizontal line in Fig. A.1). With these results, we have verified that $p_{av}(L) \simeq p_c$ for the cases with higher l_c (3 Δ in 2D and 2Δ in 3D). This result can be extended to the cases of $l_c = 2\Delta$ in 2D and of $l_c = 1.5\Delta$ in 3D, that have smaller finite size effects (due to the lower l_c/L ratio).

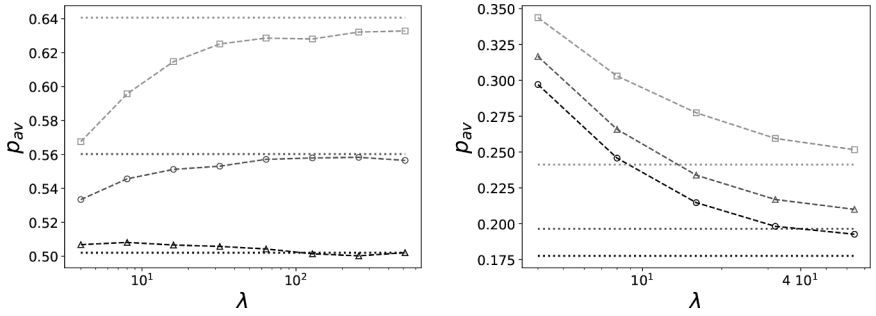

Fig. A2. Average percolation threshold p_{av} as function of the subsample size λ. (Left): 2D, $l_c = 3\Delta$. (Right): 3D, $l_c = 2\Delta$. (△): High; (∘): Intermediate; and (□): Low connectivity structure type. The dotted line is a representation of the asymptotic value for $\lambda \to \infty$.

References

Allard, D., 1993. On the connectivity of two random set models: the truncated gaussian and the boolean. Quant. Geolo. Geostat. 5, 467–478. https://doi.org/10.1007/978-94-011-1739-5_37.

Attinger, S., 2003. Generalized coarse graining procedures for flow in porous media. Comput. Geosci. 7, 253–273. https://doi.org/10.1023/B:COMG.0000005243.73381.e3.

Bernabé, Y., Mok, U., Evans, B., Herrmann, F.J., 2004. Permeability and storativity of binary mixtures of high- and low-permeability materials. J. Geophys. Res. Solid Earth 109 (B12). https://doi.org/10.1029/2004JB003111.

Boschan, A., Noetinger, B., 2012. Scale dependence of effective hydraulic conductivity distributions in 3D heterogeneous media: a numerical study. Transp. Porous Media 94 (1), 101–121. https://doi.org/10.1007/s11242-012-9991-2.

Colecchio, I., Boschan, A., Otero, A.D., Noetinger, B., 2020. On the multiscale characterization of effective hydraulic conductivity in random heterogeneous media:

a historical survey and some new perspectives. Adv. Water Resour. 140, 103594. https://doi.org/10.1016/j.advwatres.2020.103594.
Dagan, G., 1989. Flow and Transport in Porous Formations. Springer-Verlag GmbH & Co. KG. https://doi.org/10.1007/978-3-642-75015-1
Dagan, G., Fiori, A., Jankovic, I., 2013. Upscaling of flow in heterogeneous porous formations: critical examination and issues of principle. Adv. Water Resour. 51, 67–85. https://doi.org/10.1016/j.advwatres.2011.12.017.35th Year Anniversary Issue
De Wit, A., 1995. Correlation structure dependence of the effective permeability of heterogeneous porous media. Phys. Fluids 7 (11), 2553–2562. https://doi.org/10.1063/1.868705.
Dykaar, B.B., Kitanidis, P.K., 1992. Determination of the effective hydraulic conductivity for heterogeneous porous media using a numerical spectral approach: 2. Results. Water Resour. Res. 28 (4), 1167–1178. https://doi.org/10.1029/91WR03083.
Efros, A.L., Shklovskii, B.I., 1976. Critical behaviour of conductivity and dielectric constant near the metal-non-metal transition threshold. Physica Status solidi (b) 76 (2), 475–485. https://doi.org/10.1002/pssb.2220760205.
Fenton, G., Griffiths, D., 1993. Statistics of block conductivity through a simple bounded stochastic medium. Water Resour. Res. 29, 1825–1830. https://doi.org/10.1029/93WR00412.
Fleckenstein, J., Fogg, G., 2008. Efficient upscaling of hydraulic conductivity in heterogeneous alluvial aquifers. Hydrogeol. J. 16, 1239–1250. https://doi.org/10.1007/s10040-008-0312-3.
Gelhar, L.W., 1986. Stochastic subsurface hydrology from theory to applications. Water Resour. Res. 22 (9S), 135S–145S. https://doi.org/10.1002/9781118782088.ch12.
Godoy, V.A., Zuquette, L.V., Gmez-Hernndez, J.J., 2018. Stochastic analysis of three-dimensional hydraulic conductivity upscaling in a heterogeneous tropical soil. Comput. Geotech. 100, 174–187. https://doi.org/10.1016/j.compgeo.2018.03.004.
Guin, A., Ritzi Jr., R.W., 2008. Studying the effect of correlation and finite-domain size on spatial continuity of permeable sediments. Geophys. Res. Lett. 35 (10) https://doi.org/10.1029/2007GL032717.
Harbaugh, A.W., 2005. MODFLOW-2005, The US Geological Survey Modular Ground-Water Model: The Ground-Water Flow Process. https://doi.org/10.3133/tm6A16.
Harter, T., 2005. Finite-size scaling analysis of percolation in three-dimensional correlated binary Markov chain random fields. Phys. Rev. E 72, 026120. https://doi.org/10.1103/PhysRevE.72.026120.
Hashin, Z., Shtrikman, S., 1962. A variational approach to the theory of the effective magnetic permeability of multiphase materials. J. Appl. Phys. 33 (10), 3125–3131. https://doi.org/10.1063/1.1728579.
Hunt, A., Idriss, B., 2009. Percolation-based effective conductivity calculations for bimodal distributions of local conductances. Philos. Mag. 89, 1989–2007. https://doi.org/10.1080/14786430802660431.
Hunt, A.G., 1998. Upscaling in subsurface transport using cluster statistics of percolation. Transp. Porous Media 30 (2), 177–198. https://doi.org/10.1023/A:1006534922791.
Hunt, A.G., Sahimi, M., 2017. Flow, transport, and reaction in porous media: percolation scaling, critical-path analysis, and effective medium approximation. Rev. Geophys. 55 (4), 993–1078. https://doi.org/10.1002/2017RG000558.
Jankovic, I., Maghrebi, M., Fiori, A., Dagan, G., 2017. When good statistical models of aquifer heterogeneity go right: the impact of aquifer permeability structures on 3D flow and transport. Adv. Water Resour. 100, 199–211. https://doi.org/10.1016/j.advwatres.2016.10.024.
King, P., Buldyrev, S., Dokholyan, N., Havlin, S., Lee, Y., Paul, G., Stanley, H., Vandesteeg, N., 2001. Predicting oil recovery using percolation theory. Pet. Geosci. 7 https://doi.org/10.1144/petgeo.7.S.S105.
King, P.R., Andrade Jr., J.S., Buldyrev, S.V., Dokholyan, N., Lee, Y., Havlin, S., Stanley, H.E., 1999. Predicting oil recovery using percolation. Physica A 266 (1), 107–114. https://doi.org/10.1016/S0378-4371(98)00583-4.
Knudby, C., Carrera, J., 2005. On the relationship between indicators of geostatistical, flow and transport connectivity. Adv. Water Resour. 28 (4), 405–421. https://doi.org/10.1016/j.advwatres.2004.09.001.
Knudby, C., Carrera, J., Bumgardner, J.D., Fogg, G.E., 2006. Binary upscaling the role of connectivity and a new formula. Adv. Water Resour. 29 (4), 590–604. https://doi.org/10.1016/j.advwatres.2005.07.002.
Le Ravalec, M., Noetinger, B., Hu, L.Y., 2000. The FFT moving average (FFT-MA) generator: an efficient numerical method for generating and conditioning Gaussian simulations. Math. Geol. 32 (6), 701–723. https://doi.org/10.1023/A:1007542406333.
Liao, Q., Lei, G., Zhang, D., Patil, S., 2019. Analytical solution for upscaling hydraulic conductivity in anisotropic heterogeneous formations. Adv. Water Resour. 128, 97–116. https://doi.org/10.1016/j.advwatres.2019.04.011.
Linde, N., Renard, P., Mukerji, T., Caers, J., 2015. Geological realism in hydrogeological and geophysical inverse modeling: a review. Adv. Water Resour. 86 https://doi.org/10.1016/j.advwatres.2015.09.019.
Mariethoz, G., Caers, J., 2014. Multiple-Point Geostatistics: Stochastic Modeling with Training Images. John Wiley & Sons. https://doi.org/10.1002/9781118662953.
Masihi, M., Gago, P., King, P., 2016. Estimation of the effective permeability of heterogeneous porous media by using percolation concepts. Transp. Porous Media 114. https://doi.org/10.1007/s11242-016-0732-9.
Masihi, M., King, P.R., 2012. Percolation approach in underground reservoir modeling. Water Resources Management and Modeling. IntechOpen. https://doi.org/10.5772/36458.chapter 12
Maxwell, J.C., 1873. A Treatise on Electricity and Magnetism, 1. Oxford: Clarendon Press. https://doi.org/10.1038/007478a0.
Neuweiler, I., Vogel, H.-J., 2007. Upscaling for unsaturated flow for non-gaussian heterogeneous porous media. Water Resour. Res. 43 (3) https://doi.org/10.1029/2005WR004771.
Nurafza, P., King, P., Masihi, M., 2006. Facies Connectivity Modelling: Analysis and Field Study. SPE-100333-MS. https://doi.org/10.2523/100333-MS.
Oriani, F., Renard, P., 2014. Binary upscaling on complex heterogeneities: the role of geometry and connectivity. Adv. Water Resour. 64, 47–61. https://doi.org/10.1016/J.ADVWATRES.2013.12.003.
Paleologos, E., Neuman, S.P., Tartakovsky, D., 1996. Effective hydraulic conductivity of bounded, strongly heterogeneous porous media. Water Resour. Res. 32, 1333–1341. https://doi.org/10.1029/95WR02712.
Pardo-Igúzquiza, E., Dowd, P.A., 2003. CONNEC3D: a computer program for connectivity analysis of 3D random set models. Comput. Geosci. 29 (6), 775–785. https://doi.org/10.1016/S0098-3004(03)00028-1.
Pozdniakov, S., Tsang, C.-F., 2004. A self-consistent approach for calculating the effective hydraulic conductivity of a binary, heterogeneous medium. Water Resour. Res. 40 (5) https://doi.org/10.1029/2003WR002617.
Renard, P., Allard, D., 2013. Connectivity metrics for subsurface flow and transport. Adv. Water Resour. 51, 168–196. https://doi.org/10.1016/j.advwatres.2011.12.001.35th Year Anniversary Issue
Romeu, R.K., Noetinger, B., 1995. Calculation of internodal transmissivities in finite difference models of flow in heterogeneous porous media. Water Resour. Res. 31 (4), 943–959. https://doi.org/10.1029/94WR02422.
Rongier, G., Collon, P., Renard, P., Straubhaar, J., Sausse, J., 2016. Comparing connected structures in ensemble of random fields. Adv. Water Resour. 96 https://doi.org/10.1016/j.advwatres.2016.07.008.
Sanchez-Vila, X., Guadagnini, A., Carrera, J., 2006. Representative hydraulic conductivities in saturated groundwater flow. Rev. Geophys. 44 (3) https://doi.org/10.1029/2005RG000169.
Stauffer, D., Aharony, A., 1994. Percolation Theory: An Introduction, Vol. 46. https://doi.org/10.1063/1.2808877.
Tyukhova, A.R., Willmann, M., 2016. Connectivity metrics based on the path of smallest resistance. Adv. Water Resour. 88, 14–20. https://doi.org/10.1016/j.advwatres.2015.11.014.
Vassena, C., Cattaneo, L., Giudici, M., 2010. Assessment of the role of facies heterogeneity at the fine scale by numerical transport experiments and connectivity indicators. Hydrogeol. J. 18, 651–668. https://doi.org/10.1007/s10040-009-0523-2.
Western, A.W., Blschl, G., Grayson, R.B., 2001. Toward capturing hydrologically significant connectivity in spatial patterns. Water Resour. Res. 37 (1), 83–97. https://doi.org/10.1029/2000WR900241.
Wiener, O., 1912. Die theorie des mischkorpers für das feld der stationaren stromung abh sach. Ges Wiss Math Phys K 32 (509).
Zarlenga, A., Fiori, A., 2015. Advective transport through three-dimensional anisotropic formations of bimodal hydraulic conductivity. Transp. Porous Media 107, 573–593. https://doi.org/10.1007/s11242-015-0455-3.
Zarlenga, A., Jankovi ć, I., Fiori, A., Dagan, G., 2018. Effective hydraulic conductivity of three-dimensional heterogeneous formations of lognormal permeability distribution: the impact of connectivity. Water Resour. Res. 54 (3), 2480–2486. https://doi.org/10.1002/2017WR022141.
Zinn, B., Harvey, C.F., 2003. When good statistical models of aquifer heterogeneity go bad: a comparison of flow, dispersion, and mass transfer in connected and multivariate gaussian hydraulic conductivity fields. Water Resour. Res. 39 (3) https://doi.org/10.1029/2001WR001146.